

Enhanced reliability of Sn–Ag–Bi–In joint under electric current stress by adding Co/Ni elements

Youngseok Kim · Shijo Nagao · Tohru Sugahara · Katsuaki Suganuma · Minoru Ueshima · Hans-Juergen Albrecht · Klaus Wilke · Joerg Strogies

Received: 25 March 2014 / Accepted: 3 May 2014 / Published online: 11 May 2014
© Springer Science+Business Media New York 2014

Abstract In this paper, we studied the reliability of Cu joint with a Sn–Ag–Bi–In (SABI) lead-free solder under a high electric current stress with or without trace amounts of Co and/or Ni as grain refiners. Electromigration (EM) caused critical failure of the soldered structure at current densities exceeding 10 kA/cm^2 , over $100 \text{ }^\circ\text{C}$. Because of the anisotropic diffusion coefficients along the *ab* and *c* axis of β -Sn tetragonal crystal, the EM resistance of the joints depended on the grain size and their orientation. The observation of microstructure with electron backscatter diffraction revealed that the grain with the addition Co and/or Ni becomes much finer than that without any additive resulting in, an improved EM resistance. The best alloy in the present our study is SABI containing 0.1 wt% Co, exhibiting a lifetime twice larger than that with SABI. The improvements of EM reliability by these additives are significantly different depending on diffusivity of the refiner elements.

1 Introduction

Because of recent regulations such as RoHS, the use of lead-free solders in electronics packaging has become an industrial standard. Sn–Ag–Cu alloys, e.g., SAC305, have been widely adopted as a reliable replacement for Pb–Sn eutectic solders. However, the melting temperature of SAC305 is $217 \text{ }^\circ\text{C}$, which is $34 \text{ }^\circ\text{C}$ higher than that of the eutectic Pb–Sn solder. The higher melting point requires that existing soldering equipment be modified and often causes unexpected thermal damage to soldered electronic components. The demand for low-temperature lead-free solders remains high in the industry to date. The leading candidates are the Sn–Ag–Bi–In (SABI) alloys, e.g. SABI334 with the melting point of $207 \text{ }^\circ\text{C}$, exhibiting excellent thermal and mechanical properties [1–3].

Nevertheless, the continuous miniaturization of electronic devices requires finer interconnections, resulting in higher electrical current density at these interconnections. This higher current stress sometimes hinders the reliability even for SABI solders because both Ag and In are well-known elements susceptible to electromigration (EM) [4], an enhanced massive migration of metal atoms along the direction of strong electron flow. EM significantly changes the microstructure of the solder joint, which may form voids, crack, massive IMC, whiskers, and dissolution of under-bump metallization (UBM) layers. These microstructure changes lead to early failure of the soldered joints, with serious impacts on the reliability of electronic devices.

The previous studies have reported on the EM phenomena for various solders, i.e., Sn–Cu, Sn–In, Sn–Ag–Cu, and Sn–Bi. These report pointed out the importance of controlling crystallographic orientation of Sn [5]. These Sn-based solders have body-centered tetragonal (BCT)

Y. Kim · S. Nagao (✉) · T. Sugahara · K. Suganuma
ISIR, Osaka University, 8-1 Mihogaoka, Ibaraki,
Osaka 567-0047, Japan
e-mail: shijo.nagao@sanken.osaka-u.ac.jp

M. Ueshima
Taguchi Laboratory, Senju Metal Industry Co., Ltd.,
Tokyo 120-8555, Japan

H.-J. Albrecht · K. Wilke · J. Strogies
Siemens AG, Corporate Technology, Siemensdamm 50,
13629 Berlin, Germany

structures because of the β -Sn crystal lattice ($a = b = 0.583$ nm; $c = 0.318$ nm). Because of the BCT structure of Sn-based alloys, their material properties are often anisotropic, including the diffusivities of metal atoms in the β -Sn matrix [6, 7]. For example, in the BCT lattice, Cu atoms diffuse 1,000 times faster along the c axis than along the a axis [8, 9]. This also leads EM in the Sn-matrix to be anisotropic. The grain boundary of Sn, on which the diffusion becomes discontinuous, can act as an effective diffusion barrier for Cu migration under the current stress. Thus, controlling the microstructure of Sn grains is a key to improving EM reliability in these materials [10, 11]. If solder grains after reflow treatment become comparable to the size of the soldered joint, which sometimes occurs, the EM reliability critically depends on the c -axis orientation of those large grains [6]. For the purposes of improving EM reliability, solder should consist of many small Sn grains randomly oriented. In such case, the fast diffusion path along the a -axis is disturbed by grain boundaries. Several groups have already reported improving the lifetime of soldered joints by refining the microstructure of reflowed solders [6, 7].

A trace amount of metal additives is commonly employed in refinement of metals. The refiners with high melting temperatures act to inhibit grain growth during crystallization by becoming extra nucleation sites or by grain boundary pinning. This can be also applicable to refine Sn microstructure. An appropriate refiner to SABI can refine in the SABI microstructure after reflow resulting in, improving the lifetime of the soldered joints under high electric current.

The present study focuses on improving the EM resistance of SABI solder by adding Co and/or Ni to refine the microstructure. To examine the EM resistance, we applied high electric currents (~ 10 kA/cm²) to a SABI joint and refined SABI solder joints, by observing the changes in microstructure by scanning electron microscopy (SEM) with electron backscattering diffraction (EBSD) analysis. It was found that the addition of 0.1 wt% Co to SABI exhibit excellent EM resistance. The soldered joint exhibited twice-longer lifetime than that with original SABI, due to the well-refined microstructure.

2 Experimental

Lead-free solders were prepared from SABI (Sn—3 wt% Ag—3 wt% Bi—4 wt% In) alloys with additives of Co (0.1 wt%), Ni (0.2 wt%), and Co/Ni (both 0.1 wt%). These four alloys, referred to as SABI, SABI + Co, SABI + Ni, and SABI + NiCo, respectively, were processed into type-II solder powder balls with an average radius of <325 μ m and then mixed into a conventional flux (Senju Metal

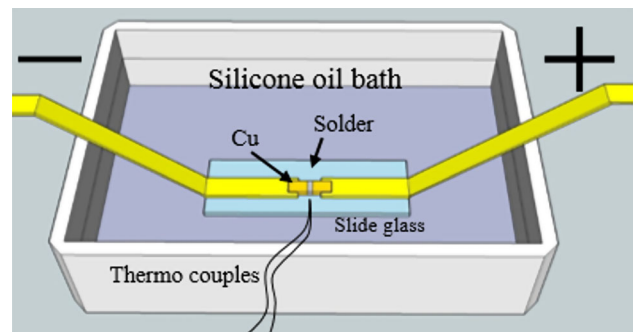


Fig. 1 Schematic of experimental setup for EM testing of soldered joints

Industry Co., Ltd., Tokyo, Japan). To prevent current crowding and to assure homogeneous current density, we soldered the joint using a linear bar structure with a rectangular cross-section [10]. The entire soldering procedure, from assembly to post-assembly, followed typical industrial reflow processes for Pb-free solders: the temperature profile, peaking at 230 ± 5 °C, and cooling in air. To evaluate EM resistance, we applied high current stress to each bonded sample using the setup shown in Fig. 1. Using a DC power supply, a constant DC current of 20 A was applied through the Cu wires, connected at both the ends of the joint samples. The applied current was determined to be 10 kA/cm². To detect EM damage and failure, the voltage and current were continuously monitored and recorded. During testing, each solder joint specimen was dipped in a silicon oil bath to prevent changes in temperature and environmental influence from the atmosphere. A K-type thermo-couple measured the temperatures of the joint and oil, which increased from Joule heating. The oil bath was placed on a hot plate at 100 ± 2 °C; during testing, the measured temperature of the oil on the sample surface was ~ 160 °C. This temperature is likely much higher than the operating temperatures of most electronic devices, making our experimental conditions suitable for an accelerated EM test. Before the tests, we measured the cross-sectional area of each joint with a micrometer. To assess the changes in microstructure of the solder joint, randomly selected samples were evaluated using back-scattered scanning electron microscopy (BS-SEM; HITACHI SU-8020, Japan). After being encased in epoxy, each cross-section was polished mechanically and then by an Ar⁺ ion-beam polisher (SM-09010; JEOL, Japan). To examine the crystallographic orientation of the grains, an electron back-scattered diffraction system (EBSD; TSL crystallography, USA) was used; these data were analyzed using TSL OIMTM 6.0 software. The compositions of the IMCs were determined using an electron probe micro analyzer (EPMA; JXA-8800, JEOL, Japan).

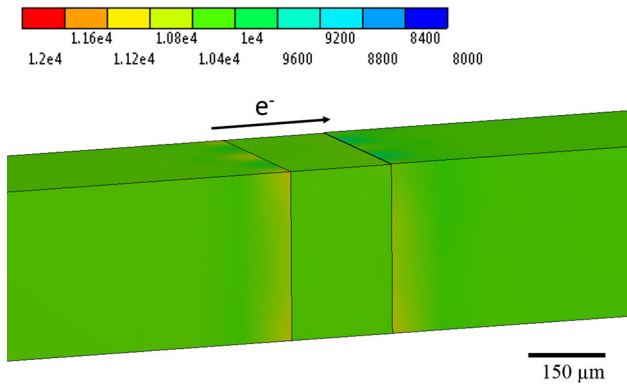


Fig. 2 Current-density distribution, calculated by FEA

3 Results and discussion

Figure 2 shows the results of finite element analysis (FEA), certifying that the electric current density of the SABI solder body is uniform between the Cu/SABI/Cu layers. The standard deviation of the current density in the solder part is $<1\%$. Considering the numerical error in the calculations, the current density in the solder material is homogeneous, with no crowded current. The variation in the copper electrodes is about 3% , caused by different electric resistance. This contrasts to the most of ball grid array (BGA) interconnections that have an unevenly distributed current density, crowding the current between the solder ball and the under-bump material (UBM) layers; the current density of a crowded region can be hundreds times

higher than that in other region of micron-size solder ball [5]. Most of the failures occurred within the crowded regions. As we confirmed in the FEA analysis, the rectangular samples had no current crowding, making it easier for us to observe EM phenomena in the bar sample than in the BGA solder joints.

Figure 3 shows cross-sectional BSE-SEM images of the interface of the Cu electrode and solder joint. At that interface, a scalloped ~ 5 to $10\ \mu\text{m}$ n- Cu_6Sn_5 IMC layer formed along with a thin Cu_3Sn layer in Fig. 3a. Micron-sized n- Cu_6Sn_5 and AgIn_2 IMCs were randomly distributed in the β -Sn matrix [12]. Small amounts of additional Co, Ni, and Ni + Co atoms did not significantly affect the microstructure or IMC thickness. However, Ni formed IMCs with both Sn and Cu. Figure 3c, d, in which the solder only contained Ni additives, shows a very thin $\text{Cu}_3(\text{Sn}, \text{Ni})$ layer between the Cu and $(\text{Cu}, \text{Ni})_6\text{Sn}_5$ layer; furthermore, $(\text{Cu}, \text{Ni})_6\text{Sn}_5$ partially infiltrated the β -Sn matrix. Unfortunately, in BSE-SEM images it is hard to distinguish the two kinds of IMCs, but the shape of the IMC layer clearly changed with the Co additive content. Figure 3b, d shows thorn-bush-like structure of the IMCs, as well as the $\text{Cu}_6(\text{Sn}, \text{Co})_5$ layer between the solder and Cu. EPMA analysis detected significant amounts of Co in the IMC layer. We believe that, Co atoms in the liquid solder and the interface to Cu substrate acted as extra nucleation sites, interrupting the grain growth of Sn matrix at solidification. The compositions of the IMC were confirmed by EPMA quantitative analysis.

Figure 4 shows the EBSD analysis of the four unstressed solder joints. The colors in Fig. 4 indicate the grain

Fig. 3 Cross-sectional BSE-SEM images: **a** SABI, **b** SABI + Co, **c** SABI + Ni and **d** SABI + NiCo

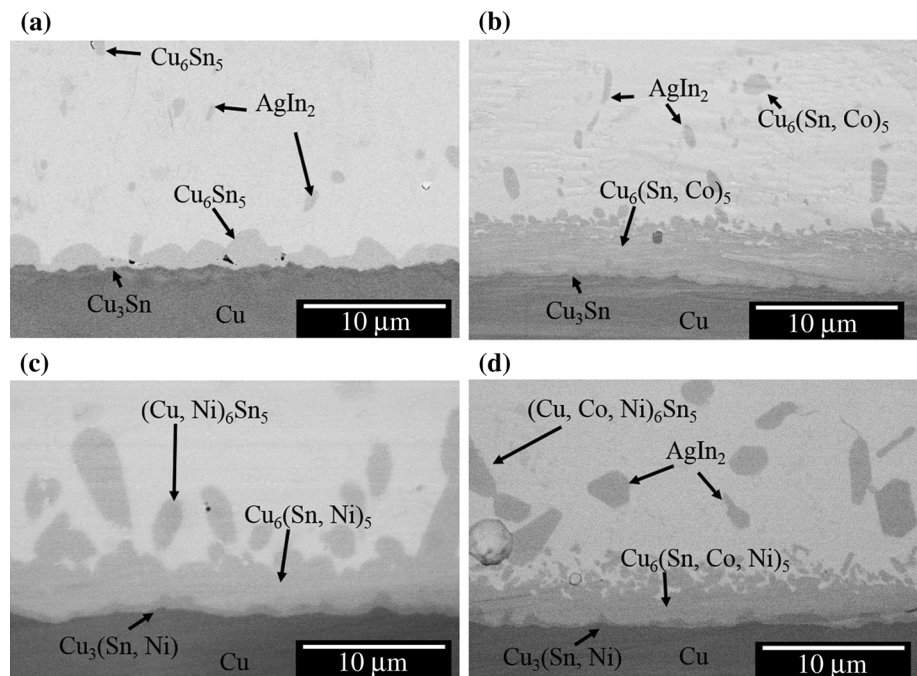


Fig. 4 EBSD analysis of the microstructures of the as-reflowed solder joints. **a** SABI, **b** SABI + Co, **c** SABI + Ni and **d** SABI + NiCo

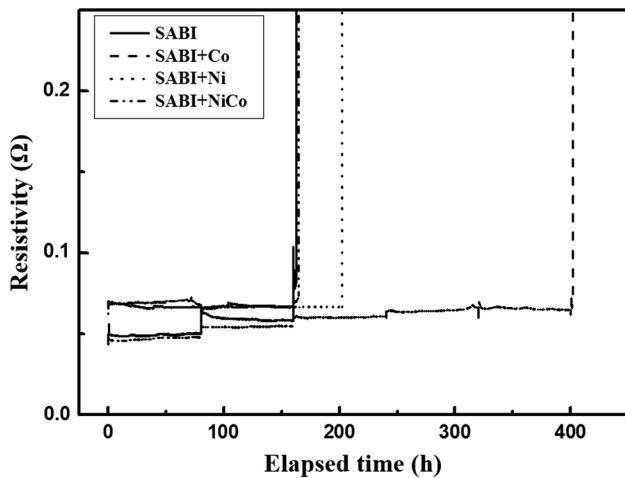
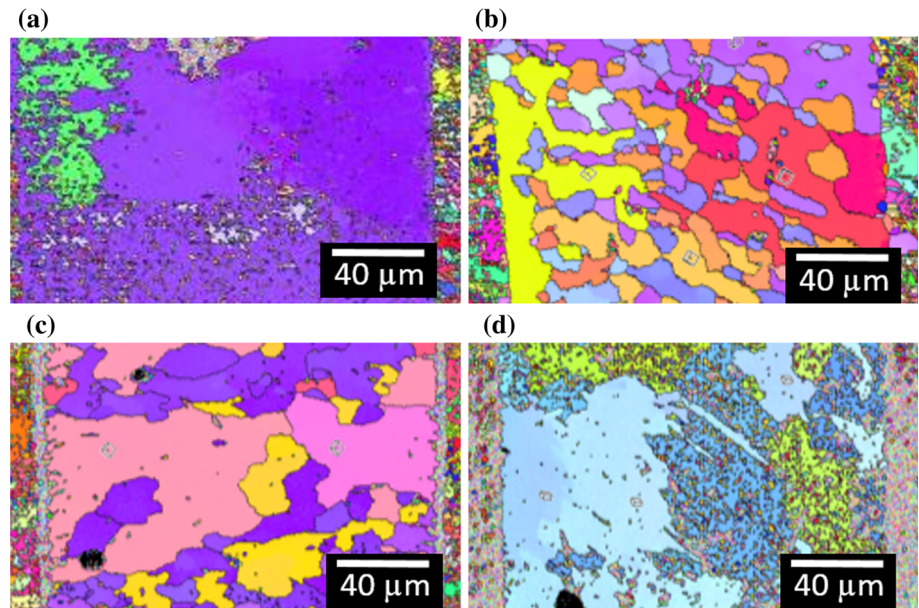


Fig. 5 Average lifetimes of the solder joints, measured by assessing electric resistivity under high-current stress at a constant temperature (100 °C)

orientation. For SABI (Fig. 4a), the β -Sn matrix consists of large Sn grains. In this case, the c axis orientations of some of the large β -Sn grains were almost parallel with the direction of electron flow, and the micron-sized IMCs were located in the Sn grain matrix. Such large grains appeared in SABI + Ni (Fig. 4c) and SABI + NiCo (Fig. 4d) as well, but several of them have tilted c axis. The Cu may have dissolved quickly in grains with a c axis parallel to the electron flow direction. SABI + Co (Fig. 4b) had especially small grains with a tilted c axis. The samples with Co and Ni additives had smaller grain size and distributed crystal axes, indicating their usefulness in refining the grains.

Figure 5 shows the electrical resistivity over time for the four solder alloys, done to assess their average joint

lifetime. These samples were placed in a silicon oil bath at 100 °C to maintain a constant environment while applying a current density of 10 kA/cm². The resistance was calculated by monitoring the voltage and current over time. The average lifetime of the five SABI samples was $\sim 159 \pm 12$ h, comparable to values in the literature; note that the In content in our solders was 4 wt% higher than those in Wu and Sun [13]. The SABI with Ni and NiCo had average failure times of ~ 200 h. The average lifetime of the SABI + Co samples was almost double those of other solder alloys, indicating that the microstructural refinement by Co addition enhanced the lifetime.

Figure 6 shows BSE-SEM images of the solder alloys across the anode and cathode after current stressing. These images show that EM caused microstructural changes, revealing the formation of voids, Cu dissolution on the cathode side, and IMC growth on the anode. In SABI (Fig. 6a), large voids formed, while in SABI + Ni (Fig. 6c) and SABI + NiCo (Fig. 6d), huge cracks spread along the cathode side along the Cu interface. SABI + NiCo also had voids in the β -Sn matrix near the cathode. SABI + Co (Fig. 6b) had fewer voids on the cathode side and less IMC growth on the anode side. Adding Co increased the lifetime and changed its microstructural evolution, indicating that Co enhanced the lifetime by stopping diffusion of Cu and Sn in the Sn matrix. While Ni refined the grain microstructure, it did not enhance the lifetime.

This difference in the results of Co and Ni additives can be explained by comparing the diffusion coefficients of Ni and Co in the Sn matrix. The diffusion coefficient D_{Cu} when parallel to the c axis is 2×10^{-6} at 25 °C and when

Fig. 6 Cross-sectional BSE-SEM images of solder-joint microstructures on the cathode and anode sides, after current stressing. **a** SABI 160 h, **b** SABI + Co 240 h, **c** SABI + Ni 200 h and **d** SABI + NiCo 200 h

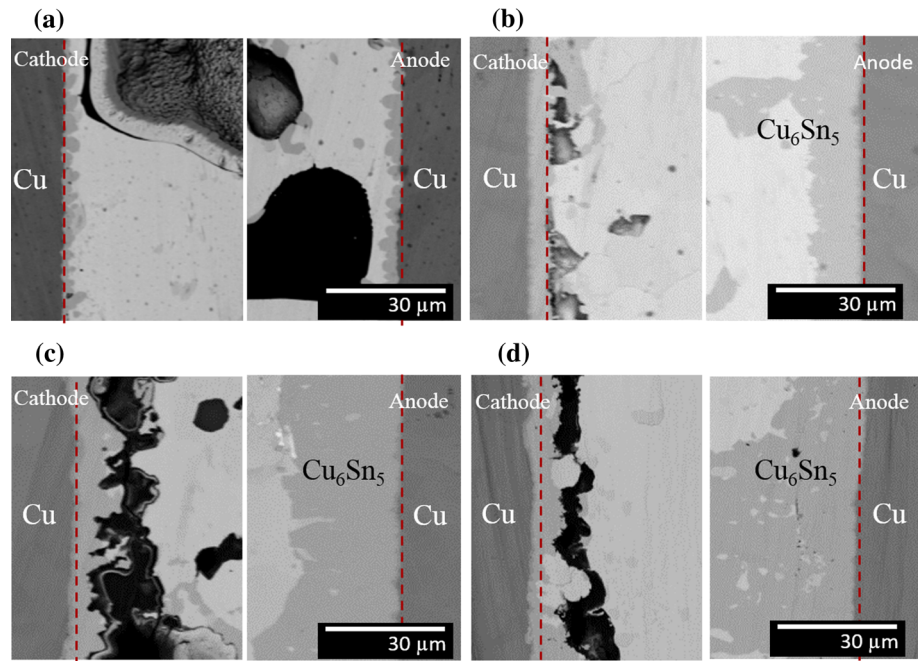
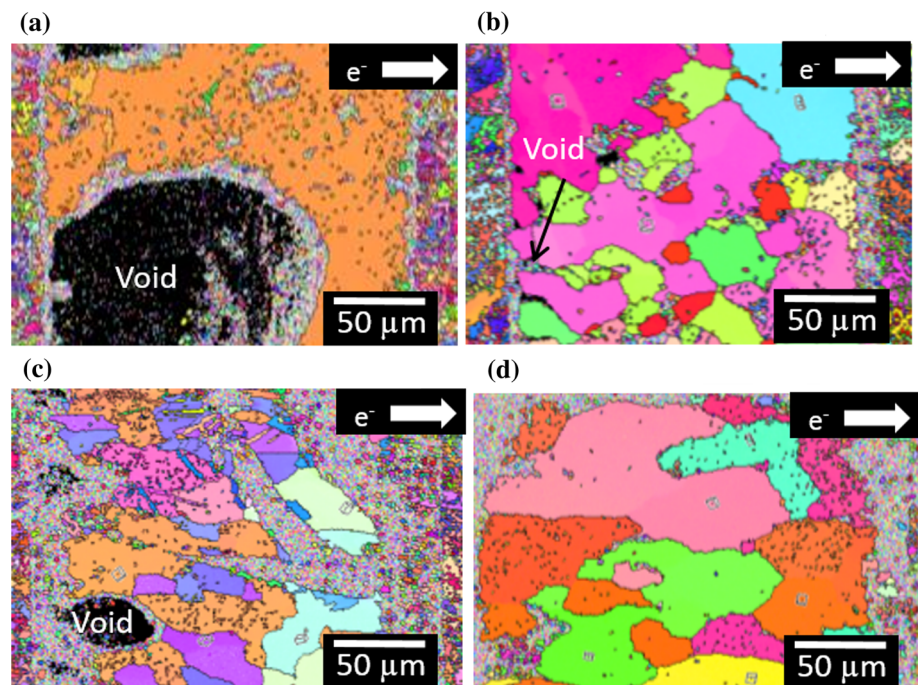


Fig. 7 EBSD analysis of the solder joints after high-current stressing. **a** SABI 160 h, **b** SABI + Co 240 h, **c** SABI + Ni 160 h and **d** SABI + NiCo 160 h



perpendicular is 2.4×10^{-3} at 140–230 °C [14]. Contrasting to highly anisotropic D_{Cu} , D_{Ni} and D_{Co} are independent from the c axis of Sn matrix; 2×10^{-2} and 5.5, respectively. These differences affect the diffusion velocity during EM: Co can act like a diffusion barrier, especially in the grain boundaries and IMC layers between the solder and Cu. However, Ni aids the diffusion of Cu and produces composite IMCs with Cu and Sn [15]. Thus, 0.1 wt% Co

addition result in best EM resistance in our study because of the slowest atomic diffusion in Sn matrix.

Figure 7 shows the EBSD analysis of the current-stressed solder alloys. Generally, in all samples the IMCs increased in volume over time during current stressing. Void formation and growth of IMCs between the solder and Cu pad are normal reactions that often occur during EM. Figure 7a, c, d shows the EBSD analysis of SABI,

SABI + Ni, and SABI + NiCo, respectively, after EM testing for 160 h, while Fig. 7b shows SABI + Co after 240 h. These results show that well-refined, randomly distributed grain orientation can reduce damage by current stress. Atomic diffusion in β -Sn matrix is anisotropic, especially when the c axis is parallel to the direction of electron interstitial diffusion of Cu. In Fig. 7a, the c axis of Sn in the SABI solder was almost parallel to electron flow, causing Cu to dissolve quickly on the cathode side and causing large Cu–Sn IMCs to form near both the cathode and anode sides. For SABI + Co, its c axis was also nearly parallel to the electron flow. The twice-longer lifetime of SABI + Co was caused by its smaller grain size and tilted c axis. Thus, the refined microstructure of the Sn matrix suppressed Cu dissolutions and IMC growths disturbed by the grain boundaries. Based on these results, we conclude that the EM failure of the SABI, SABI + Co, SABI + Ni, and SABI + NiCo solder joints was caused by crack propagations at the cathode interface and by void aggregations in the β -Sn matrix.

From our analysis, we confirm that additive refinement is a reasonable method for enhancing EM reliability in Sn-based solder joints. Nevertheless, adequate selection of the additive element requires evaluating its diffusivity under current stress.

4 Conclusion

We investigated the EM behaviors of SABI, SABI + Co, SABI + Ni, and SABI + NiCo alloys. They exhibited remarkable differences depending on the trace amounts of Co and Ni atoms. We determined the primary reason for EM failure of the solder joints was the propagation of defects between the cathodal IMCs and the solder alloys, caused by dissolution of the Cu electrode. Adding Co substantially reduced the Sn grain size. To investigate how

additional trace materials affected the alloys, the Sn grain structure was characterized using EBSD analysis. The grain size and c -axis orientation of the alloys were correlated with their EM reliability. The lifetimes and microstructural changes caused by current stress indicated that these additives were considerably effective and that their effectiveness depended on diffusivity of the corresponding element in the Sn matrix.

Acknowledgments This work was partially supported by a Grant-in-Aid for Scientific Research (S); Grant Number 24226017.

References

1. K. Suganuma, K. Niihara, T. Shotoku, Y. Nakamura, *J. Mater. Res.* **13**, 2859 (1998)
2. K.S. Kim, T. Imanishi, K. Suganuma, M. Ueshima, R. Kato, *Microelectron. Reliab.* **47**, 1113 (2007)
3. A. Yamaguchi, Y. Yamashita, A. Furusawa, K. Nishida, T. Hojo, Y. Sogo, A. Miwa, A. Hirose, K.F. Kobayashi, *Mater. Trans.* **45**, 1282 (2004)
4. C.Y. Liu, *Appl. Phys. Lett.* **75**, 58 (1999)
5. J.W. Nah, J.O. Suh, K.N. Tu, *J. Appl. Phys.* **98**, 013715 (2005)
6. Y. Wang, K.H. Lu, V. Gupta, L. Stiborek, D. Shirley, S.H. Chae, J. Im, P.S. Ho, *J. Mater. Res.* **27**, 1131 (2012)
7. H. Xie, D. Friedman, K. Mirpuri, N. Chawla, *J. Electron. Mater.* doi:10.1007/s11664-013-2667-z
8. B.F. Dyson, *J. Appl. Phys.* **38**, 3408 (1967)
9. F. Huang, *Phys. Rev. B* **91**, 479 (1974)
10. K. Lee, K.S. Kim, K. Suganuma, *J. Mater. Res.* **26**, 2624 (2011)
11. M. Lu, D. Shih, P. Lauro, C. Goldsmith, D.W. Henderson, *Appl. Phys. Lett.* **92**, 211909 (2008)
12. L.D. Chen, M.L. Huang, S.M. Zhou, *J. Alloys Compd.* **504**, 535 (2010)
13. A.T. Wu, K.H. Sun, *J. Electron. Mater.* **38**, 12 (2009)
14. E.A. Brandes, G.B. Brook, *Smithells Metals Reference Book*, 7th edn. (Butterworth-Heinemann, Oxford, 1992), pp. 13–25, table 13.2
15. D.C. Yeh, H.B. Huntington, *Phys. Rev. Lett.* **53**, 15 (1984)